ELSEVIER

Contents lists available at ScienceDirect

Chemical Engineering Journal

journal homepage: www.elsevier.com/locate/cej



Methanol production through combined carbon capture and hydrogenation: unravelling the benefits of two-step hydrogenation[★]

A. Chila ^{a,1}, A.W.N. de Leeuw den Bouter ^{a,b,e,1,2}, L. Brito ^c, A. Miquelot ^b, P. Olivier ^b, J. van der Schaaf ^{a,d,*}

- a Sustainable Process Engineering, Chemical Engineering and Chemistry, Eindhoven University of Technology, the Netherlands
- ^b Lab Hydrogen, ENGIE Lab CRIGEN, Stains, France
- c Lab Biogas, Biomass and Waste, ENGIE Lab CRIGEN, Stains, France
- ^d Eindhoven Institute for Renewable Energy Systems (EIRES), the Netherlands
- ^e The Netherlands Organisation for Applied Scientific Research (TNO), Energy & Materials Transition, Amsterdam, the Netherlands

ARTICLE INFO

Keywords: Methanol Catalysis Combined carbon capture and hydrogenation Gold catalysis Process optimization

ABSTRACT

The combined carbon capture and hydrogenation towards methanol was demonstrated using dipropylamine as carbon capture agent. Previous works highlighted the reaction to follow a complex mechanism, in which the carbamate species formed during carbon capture is hydrogenated into N-formamide species, which are subsequently hydrogenated into methanol. The rate limiting step was observed to be the second step. Therefore, this work aimed to improve the conversion of N-formamide species into methanol.

Comparing Au/ZnO, Au/MgO, Au/CeO₂, Au/ZrO₂ and Au/TiO₂ catalysts using N,N-dipropylformamide as starting material, it was concluded that the methanol productivity strongly correlates with the surface basicity of the catalyst support. This was rationalized in relation to the reaction mechanism, in which the first hydrogenation step of the formamide species is proposed to occur via a hemiaminal intermediate. While basic catalysts are required for the hydrogenation of N-formamides into methanol, the formation of N-formamides from N-carbamates requires acidic sites. Therefore, we proposed a two-step strategy within this work, using first an acidic catalyst bed (Pd/Al_2O_3), followed by a basic catalyst bed (Pd/Al_2O_3), followed by a basic catalyst bed (Pd/Al_2O_3).

The novel process configuration was compared to the state-of-the-art single step process showing the complete reaction from CO_2 captured in dipropylamine in the form of carbamate to methanol. Here, the methanol productivity was observed to increase by $\sim 100 \times$ compared to the previously proposed single step configuration.

1. Introduction

The large scale burning of fossil fuels has resulted in a significant increase in $\rm CO_2$ levels within the atmosphere, with atmospheric $\rm CO_2$ concentration nearly doubling in the last 75 years, reaching 445 ppm in 2021 compared to 212 ppm in 1958 [1]. Such continuous rise in $\rm CO_2$ levels caused by anthropogenic emissions leads to significant changes in the world's climate, and therefore poses one of the greatest challenges faced by society nowadays [2–4].

Alternatively, CO₂ could be utilized as an alternative, non-toxic and renewable carbon source instead of oil or natural gas, as catalytic

conversion of CO₂ with renewable H₂ allows for the synthesis of a wide range of products such as formic acid, methanol, methane and dimethyl ether [5–7]. Of these products, methanol is particularly interesting as it is among the top five basic chemicals worldwide in terms of annual tonnage produced and is an essential C1 building block for a multitude of products such as formaldehyde, acetic acid and olefins [8]. Methanol can also be directly used as a liquid fuel in internal combustion engines and fuel cells [9], or be further converted into gasoline [10]. Besides further processing, methanol is also investigated as a Liquid Organic Hydrogen Carrier (LOHC) due to its high hydrogen content of 12.5 wt% as proposed by Olah [11]. Hence, the hydrogenation of CO₂ towards

^{*} This article is part of a Special issue entitled: 'CCUS' published in Chemical Engineering Journal.

^{*} Corresponding author at: Sustainable Process Engineering, Chemical Engineering and Chemistry, Eindhoven University of Technology, the Netherlands. E-mail address: j.vanderschaaf@tue.nl (J. van der Schaaf).

 $^{^{1}}$ Authors contributed equally.

² Current address.

methanol is highly sought after in industry and academia [12].

However, the direct hydrogenation of CO_2 towards methanol requires high purity and high pressure CO_2 [9,13,14]. While CO_2 can be obtained through carbon capture directly from the atmosphere or industrial exhaust sources, significant energy penalties are associated with this process caused by the necessity of CO_2 separation and purification as well as solvent regeneration [6]. Besides significant energy requirements up to 85 kJ per mole of CO_2 required for solvent regeneration, the process remains economically prohibitive due to the high cost of compression and transportation of captured CO_2 [15].

In order to circumvent the high energy penalties and costs associated with amine solvent regeneration and CO_2 compression, the concept of integrated capture and conversion of captured CO_2 ($\mathrm{IC}^3\mathrm{M}$) has been widely investigated for a range of hydrocarbon products such as formic acid, CO , methane and methanol [5–7]. Freyman et al. have shown that through removal of these costly and energy intensive key process steps, the concept of $\mathrm{IC}^3\mathrm{M}$ allows for a reduction of approximately 50 % of the total energy requirement for methanol production from CO_2 [16]. Additionally, a techno-economic evaluation performed by Kothandaraman et al. also highlighted the viability of the $\mathrm{IC}^3\mathrm{M}$ approach for methanol production, determining a methanol selling price as low as \$470/t, which is cost parity to fossil-derived methanol [7].

Recent works by Kothandaraman et al. and Chila et al. have demonstrated the process to follow a two-step mechanism, with the carbamate species formed during carbon capture (blue square Fig. 1) being hydrogenated into formamides (green square), and the subsequential hydrogenation of these formamides into methanol and a secondary amine (red square) [7,17,18,20]. An overview of the overall reaction is given in Fig. 1.

These works have highlighted the hydrogenation of the intermediate formamide species to be the rate determining step, with up to 99 % of the carbamate species undergoing hydrogenation towards formamides but subsequent methanol concentrations remaining within the millimolar range [7,18–20].

Common strategies for the reduction of amides such as the formamide species formed during the first hydrogenation step, involve the utilization of overstoichiometric reductants such as hydrosilanes or hydroboranes [10]. While this approach was successfully demonstrated by Uranga et al. for the production of methanol from a wide range of formamides with high selectivity, the utilization of metal hydrides inherently results in low atom efficiencies and large waste streams [21]. Therefore, catalytic hydrogenation using molecular hydrogen is preferred.

Milstein et al. and Kothandaraman et al. reported that the addition of bases such as KOH and *t*-BuOK significantly enhances the methanol productivity over heterogenous catalysts [25,26]. This was rationalized through mechanistic studies, where it was shown that the initial hydrogenation of the formamide species occurs via the formation of a hemiaminal, with the addition of such bases facilitating the deprotonation of the intermediate hemiaminal, therefore retarding the cleavage of the C—O bond [26]. Despite these promising results, the addition of highly corrosive bases would significantly complicate the downstream

processing required to obtain high purity methanol. Therefore, this work proposes the utilization of solid bases such as ZnO, ZrO₂, CeO₂ and MgO in the form of catalysis supports to enhance the hydrogenation of the intermediate formamide species.

Besides the production of methanol being severely limited by the hydrogenation of the stable secondary formamide, previous works also highlighted the selectivity of the reaction to be challenging. The formamide species can be hydrogenated according to two mechanisms: cleavage of the C-N bond, yielding a secondary amine and methanol, and C—O cleavage yielding a tertiary amine, therefore deactivating the carbon capture amine. Heterogeneous catalysts often favour C-O cleavage, therefore deactivating the carbon capture solvent [7,18,20]. Alternatively, it has been proposed that methanol itself is the primary source of N-methylation [7,25]. C—O hydrolysis was demonstrated to be the preferred pathway over bifunctional catalysts containing acidic oxophilic metals such as Re or Mo either as catalyst supports or integrated with a common hydrogenation metal, as such acidic sites on oxophilic metals are known to activate the carbonyl group [10]. However, acidic sites are required for the formation of the formamide from carbamates [7,10,22–24]. Thus, the catalyst properties required for the first and second reaction steps are vastly different, with the first step occurring over acidic sites, and the second step occurring over basic sites. Interestingly, the work of Kothandaraman et al. already demonstrated the requirement of the presence of both acid and basic sites for selective C-N cleavage, highlighting the promising nature of TiO2, CeO₂ and Al₂O₃ supports [7]. However, the large amount of acidic sites resulted in significant solvent deactivation caused by selectivity issues. Within this work, the single step reaction as performed by e.g. Kothandaraman et al. using amphoteric supports is compared to a twostep reaction protocol, in which the carbamate hydrogenation is performed using acidic catalysts, and the formamide hydrogenation is performed using basic catalysts.

Despite promising results demonstrated by previous works, these studies also revealed severe catalyst deactivation for palladium, ruthenium and platinum based catalysts, originating from the strong interaction with carbon species such as CO and carbonates [7,18,20]. Therefore, this current work aims at the development of catalysts supported on these promising catalysts supports, combined with common hydrogenation metals demonstrating high tolerances towards carbon poisoning such as Au and Co.

Within this work, the carbon capture agent of choice is dipropylamine (DPA), a commonly used, commercially available post-combustion carbon capture agent. Efficient carbon capture was previously demonstrated for this amine, with the resulting dipropylcarbamate remaining relatively non-viscous [27,28]. This work aims to facilitate a deeper understanding into the control of product selectivity for the hydrogenation of formamides using a high-pressure continuous fixed bed flow reactor. Therefore, N,N-dipropylformamide was selected as a starting material to allow for isolation of the second hydrogenation step from the complex reaction mechanism. After optimization in terms of catalyst formulation, residence time and temperature, the optimized catalytic system is demonstrated for the combined carbon capture and

Fig. 1. Schematic overview of the reaction, based on the work of [7,18,20]. The first reaction represents the reaction between CO₂ and dipropylamine. The formed carbamate is subsequently hydrogenated to N-formamide, followed by the formation of methanol and the original carbon capture agent.

hydrogenation using dipropylamine as carbon capture amine and compared to the state-of-the-art presented in literature.

2. Experimental materials and methods

2.1. Materials

Au/TiO $_2$ (1 wt% Au) cylindrical catalyst pellets (AUROlite) were purchased from Strem Chemicals. Pd/Al $_2$ O $_3$ (1 wt% Pd), Co/Al $_2$ O $_3$ (40 wt% Co) were obtained from Thermo Scientific. Chloroauric acid trihydrate (HAuCl $_4$ ·3H $_2$ O) (99.995 %) and γ -alumina powder (99.9 %) were purchased from Sigma Aldrich. Magnesium oxide (99.95 %) was received from VWR Chemicals. Isopropanol was purchased from Boom Chemicals, while N,N-dipropylformamide (>99.9 %) was obtained from Fluorochem. Glass beads, SiC and quartz wool, used for reactor packing, were obtained from Thermo Scientific, Karl Heckt GmbH and Carl Roth respectively.

Gold standard for ICP was obtained from Fluka TraceCERT Ultra (1002 ppm). Hydrofluoric acid EMSURE (48 %), nitric acid (65 %) EMPLURA (>99.9 %), hydrochloric acid (37 %) a.c.s. reagent, sulfuric acid (98 %), dipropylamine (>99 %), Zinc Oxide powder (99.999 %), zirconia powder (99.9 %), titania (99.9 %) and ceria powder (99.9 %) were purchased from Merck Life Science.

All chemicals were used as received, handled in air and used without any additional purification. In order to prevent catalyst deactivation, the catalysts were stored under Ar in a cold and dark environment.

2.2. Catalyst preparation

Au/TiO₂ (1 wt% Au), Pd/Al₂O₃ (1 wt% Pd) and Co/Al₂O₃ (40 wt% Co) were commercially obtained. All other Au based catalysts were synthesized using deposition-precipitation with NaOH as precipitation agent. The detailed experimental protocols are described elsewhere [29-31]. Typically, an aqueous suspension (10 g/L) was prepared with the commercial catalyst support, and heated until 70 °C. Proper Au precursor dispersion was ensured through dropwise addition using a burette. Following the formation of a stable suspension, NaOH was added dropwise until the desired pH was obtained. Prior to synthesis, the Point of Zero Charge (PZC) was determined using titration. The resulting mixture was stirred for 1 h, shielded from light using aluminum foil to prevent bulk precipitation due to light exposure. Residual chlorine was removed through washing with D.I. water, until no precipitation was observed when mixing the filtrate with Ag(NO)₃. The prepared catalysts were subsequently dried at 120 $^{\circ}\text{C}$ for 24 h, and calcined in air at 250 °C for 4 h, followed by reduction for 3 h in a 10 vol% H₂ stream at a temperature of 300 °C using a 2 °C /min ramp rate [29-31]. All commercial support materials were calcined at 500 °C for 24 h, followed by crushing and sieving to the correct size fraction prior to catalyst synthesis. The Au/TiO₂ catalyst was obtained in the form of extrudates, which were crushed and sieved prior to usage. The resulting Au loadings were determined with ICP-OES, the desired loading was 1 wt%.

2.3. Activity testing and product analysis

Carbon capture experiments were conducted at ambient conditions over a time period of at least 3 h, as described in [18]. Combined carbon capture and hydrogenation experiments and formamide hydrogenation experiments were performed at elevated pressure in a stainless steel packed bed reactor, described elsewhere [18,32].

The gaseous reaction products were analyzed with a compact GC (Global Analyser Solution) equipped with a TCD detector and two-packed columns (Molsieve 5A and Rt-Q-BOND). The lower detection limit for CO was established to be 2 ppm, with further details described in [18,32].

The liquid products (alcohols, formamides and amines) were analyzed using GC-MS (GC: GC2010 plus, MS: GCMS-QP 2010 Ultra),

equipped with a packed column (DB-200). The column oven was set to an initial temperature of 50 $^{\circ}$ C, with an injection temperature of 250 $^{\circ}$ C. After an initial period at constant temperature, the oven temperature was gradually increased to 250 $^{\circ}$ C, at a ramp rate of 10 $^{\circ}$ C/min.

2.4. Catalyst characterization

Inductively Coupled Plasma – Optical Emission Spectroscopy (ICP-OES; iCAPTM PRO ICP-OES; Thermo ScientificTM) was used to obtain the Au concentrations of the fresh and spent catalysts. Samples were prepared by dissolution of 100 mg of catalyst in a mixture of concentrated HF (3 mL) and aqua regia (6 mL) at elevated temperatures up to 80 °C. Samples supported on γ -alumina were digested using a two-step protocol [33], Au was first digested in 6 mL of aqua regia at 60 °C for 2 h, followed by digestion of the γ -alumina support through the addition of 1 mL of DI water and 1 mL of concentrated $\rm H_2SO_4$ at 70 °C. After digestion, the samples were filtered and diluted using double distilled water, irrespective of using a one or two step digestion protocol.

NH $_3$ Temperature Programmed Desorption (NH $_3$ TPD; Micromeritics Autochem II) was used to determine the catalyst acidity. First, 100 mg of catalyst is degassed and dried at 200 °C for 2 h, followed by reducing at 300 °C for 60 min under a 40 mL/min 10 vol% H $_2$ /Ar flow, using a ramp rate of 5 °C/min. During this time, the TCD signals are recorded to ensure full reduction. The H $_2$ is then purged using an Ar flow for 60 min at room temperature. Next, the catalyst surface is saturated with ammonia using 2 vol% NH $_3$ /Ar at 50 °C for 60 min, followed by 60 min of flushing with Ar at a flow of 40 mL/min at remove physiosorbed ammonia. Ar was then flowed continuously with a ramp rate of 5 °C/min until a final temperature of 800 °C was reached.

 CO_2 Temperature Programmed Desorption (CO₂ TPD; Micromeritics Autochem III) was used to determine the catalyst basicity. The protocol was identical to the NH₃ TPD measurements, using a 10 vol% CO₂/He mixture and flushing with He.

 H_2 Temperature Programmed Reduction (H $_2$ TPD; Micromeritics Autochem III) was performed to study the reducibility of the Co catalysts. Here, 100 mg of catalyst was degassed and dried at 150 °C for 2 h. Afterwards, the catalyst bed was cooled to 30 °C and a 10 vol% H_2/Ar was continuously flowed at a flow rate of 50 mLn/min, with a ramp rate of 10 °C/min until a final temperature of 800 °C was reached. The outgoing gas mixture was passed through a cold trap using a liquid N_2 isopropanol slurry.

3. Results and discussion

3.1. Catalyst selection

N,N-dipropylformamide was selected as a starting material to allow for isolation of the second hydrogenation step from the complex reaction mechanism. Initially, the hydrogenation of N,N-dipropylformamide towards methanol and dipropylamine was investigated using Au/TiO2 and Co(O)/Al₂O₃ as catalyst at several temperatures, with results summarized in Table 1. Au/TiO2 was selected as previous work has demonstrated Au/Al₂O₃ to have C-O hydrolysis as the prevailing pathway [34]. Both metallic Co and CoO have been shown to catalyze the hydrogenation of gaseous CO2 towards methanol, in which the productivity and selectivity were largely dependent on the Co oxidation state and interaction with the metal oxide support [35]. For example, in the case of TiO2, the CO2 hydrogenation rate of the CoO species towards methanol was observed to be higher than the one of Co⁰ at the same conditions [36]. The Co⁰ and CoO catalysts were prepared from a commercial Co_3O_4/Al_2O_3 by controlling the reduction temperature during H₂ exposure (i.e., 320 °C and 450 °C for CoO and Co⁰, respectively). Here, two distinct peaks are visible, corresponding to the two step reduction of Co₃O₄ to CoO and the subsequent reduction of CoO to Co^0 [37].

From the experiments summarized in Table 1 it becomes evident that

Table 1 Comparison of Au/TiO₂ and Co_x/Al₂O₃ catalysts at several temperatures after 1.5 hr time-on-stream. Experimental conditions: 2.0 g catalyst, 40 bar H₂ and a total residence time of 15.7 min in a 10 vol% N,N-dipropylformamide/IPA mixture. C—N cleavage selectivity = methanol concentration * 100 / (methanol concentration + N-methyldipropylamine concentration).

Catalyst	Temperature [K]	Methanol productivity [mmol/l/g _{metal}]	C-N cleavage selectivity (%)	Product selectivity [carbon%]			
				СО	CH ₄	МеОН	DPA N-Me
Au/TiO ₂	398.15	3.52	0.07	0	0	0.065	99.93
Au/TiO ₂	423.15	8.03	0.03	0	0	0.028	99.97
Au/TiO ₂	448.15	41.1	0.09	0.04	0	0.090	99.87
CoO/Al_2O_3	398.15	0	0	0	0	0	100
CoO/Al_2O_3	423.15	0	0	0	0	0	100
CoO/Al_2O_3	448.15	0.073	0.08	0	0	0.076	99.92
Co/Al_2O_3	398.15	0.123	12.99	0	0	12.99	87.01
Co/Al ₂ O ₃	423.15	1.175	3.89	0	0	3.89	96.11
Co/Al_2O_3	448.15	0.576	2.94	3e-3	0	2.94	97.15

the methanol productivity is highly temperature dependent at a constant residence time for all catalysts studied. In case of the $\rm Au/TiO_2$ catalyst, the methanol productivity per gram of Au increases from 3.5 to 41.1 mmol/l/g_{metal} when increasing the reaction temperature from 125 °C to 175 °C. However, the major product for all temperatures is observed to be *N*-methyldipropylamine, with trace amounts of CO being produced at 175 °C. The formation of *N*-methyldipropylamine originates from the cleavage of the C—O bond in the formamide molecule, which was previously observed to often be the prevailing pathway in the presence of supported heterogeneous catalysts [7,10].

In line with previous works performed under similar operational conditions [18], no gaseous CO_2 was observed at any of the studied conditions, therefore confirming the hydrogenation reaction to occur in the condensed phase.

Besides the reactive hydrogenation products of dipropylformamide, namely carbon monoxide, MeOH and N-methyldipropylamine, also the formation of propylamine, tripropylamine, acetone and isopropyl formate is observed at all temperatures. The formation of propylamine and tripropylamine when using dipropylamine as carbon capture agent was previously reported by Chila et al. under similar reactive conditions [18]. Here, the alkylation and dealkylation of dipropylamine was proposed to occur via a Schiff base mechanism under influence of H₂ and common hydrogenation catalysts. A simplified overview of the reaction mechanism including observed side reactions is given in Fig. 2, based on the work of Chila et al. [18].

Besides amines, also the formation of significant amounts of isopropyl formate, namely, 5.4 mmol/l, 7.4 mmol/l and 8.3 mmol/l, at $125\,^{\circ}$ C, $150\,^{\circ}$ C and $175\,^{\circ}$ C respectively, is observed to form. A possible explanation for the formation of this product is the direct esterification of the N,N-dipropylformamide with the isopropanol solvent, occurring

over the TiO₂ support, resulting in the formation of the ester and dipropylamine [39]. Lastly, acetone is observed to form at all studied temperatures, with 221 mmol/l produced at 175 °C. The dehydrogenation of alcohols commonly occurs over redox sites or a pair of Lewis acid-base sites, yielding hydrogen and acetone in the case of isopropanol dehydrogenation at the temperatures studied within this work [40,41].

The Co₃O₄ catalyst did not yield any activity at the studied temperatures, while the CoO based catalyst only produced trace amounts of methanol (0.07 mmol/l/g_{metal}) at 175 °C, with no methanol productivity at lower temperatures. While the fully reduced Co⁰/Al₂O₃ catalyst was observed to be much less active than the Au/TiO₂ catalyst at all studied temperatures, with the methanol productivity rate only being 0.576 mmol/l/g_{metal} compared to 41.1 mmol/l/g_{metal}, the desired selectivity towards C—N cleavage is $\sim\!40\times$ higher. Despite the significant increase in methanol selectivity, the major product remained N-methyl-dipropylamine resulting from C—O cleavage of the formamide. Similarly to the gold-based catalyst, the production of propylamine, tripropylamine and acetone is observed, while no isopropyl formate is formed over the Al₂O₃ support.

3.2. Optimization of reactive conditions

Within Section 3.1, the undesired *N*-methylation of N,N-dipropylformamide through C—O cleavage of the N-formamide species was observed to be the prevailing pathway under the studied conditions for all catalysts. Alternatively, it has been proposed that methanol itself is the primary source of *N*-methylation [7,25]. Therefore, the rate of *N*-methylation is strongly influenced by reaction parameters such as temperature and residence time [7,18]. Experiments were performed at several temperatures and residence times for the Au/

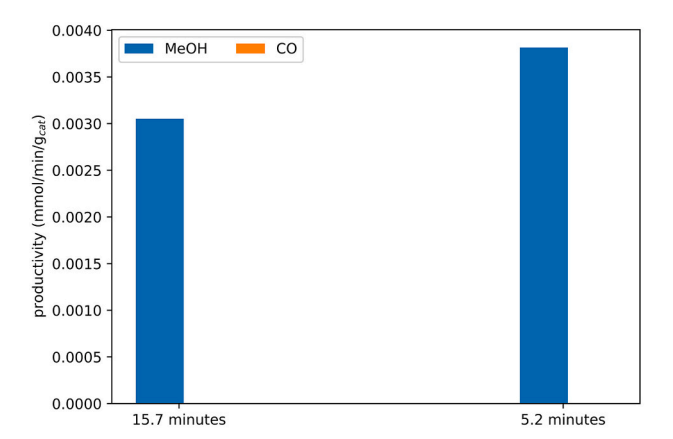
Fig. 2. Schematic overview of the reaction including side reactions. Adapted from [18].

 ${
m TiO_2}$ and ${
m Co^0/Al_2O_3}$ catalyst in order to assess the dependency of the product selectivity. The ${
m Co^0}$ oxidation state was selected due to its much higher activity compared to the other 2 Co oxidation states tested, as shown in Table 1.

In Figs. 3 and 4, the influence of a reduction in residence time under constant gas-to-liquid ratio on the methanol productivity and reaction selectivity is shown for the $\rm Au/TiO_2$ and $\rm Co^0/Al_2O_3$ catalyst respectively at 135 °C, while Figs. 3 and 4 show the influence at 175 °C. As no catalyst deactivation was observed for either catalyst, the data shown is the average observed concentration of at least 5 reactive samples taken at regular intervals.

From Figs. 3 and 4, a slight dependency with residence time becomes evident. In case of the Au/TiO2 catalyst (Fig. 1), the methanol productivity increases ~20 %, with the production of unwanted by-products such as propylamine, tripropylamine and N-methyldipropylamine decreasing upon reducing the residence time. Here, the C-N cleavage selectivity increases slightly increases by 0.02 % with decreasing the residence time from 15.7 to 5.2 min, such an increase in selectivity was previously observed by [18]. Similar trends are observed for the Cobased catalyst, with the methanol production nearly doubling. Upon comparison of the products formed by the Au versus Co-based catalyst depicted in Figs. 3 and 4, the Co-based catalyst produces significantly higher amounts of acetone through the dehydration of the isopropanol solvent independent of the residence time, with the acetone productivity of the Au-based catalyst being approximately 5 times lower at a residence time of 5.2 min. Besides the production of acetone, also the formation of propylamine and tripropylamine is observed for both active metals. While the formation of these products was shown to be inevitable due to being attributed to a combination of thermal and catalytic effects in previous works [18], the observed reactions rates differ significantly between the two studied catalysts, with the production rate of the Au supported catalyst being approximately 1.5 times higher for propylamine and 6.2 times for tripropylamine. A possible explanation for this is the direct esterification of the N,N-dipropylformamide. As was previously observed in Section 3.1, the Co/Al₂O₃ catalyst does not catalyze the direct esterification of the formamide species with the solvent, which results in the formation of an ester and dipropylamine. While the conversion of both catalysts is similar, the esterification reaction causes the concentrations of dipropylamine within the reactor to be significantly higher in case of the Au/TiO2 and therefore also the formation of propylamine and tripropylamine.

Upon increasing the temperature to 175 °C, as depicted in Figs. 5 and 6, similar trends are observed as at 135 °C when reducing the residence time, meaning an increase in methanol productivity through a decrease of *N*-methylation. Reducing the residence time increases the C—N cleavage selectivity from 0.1 % to 0.58 % and 3.6 % to 8.9 % for the Au/ TiO_2 and Co/Al_2O_3 catalysts, respectively.



Besides an increase in all products formed, the increase in temperature also results in the formation of CO. Increasing the temperature from 135 $^{\circ}\text{C}$ to 175 $^{\circ}\text{C}$ at a residence time of 5 min results in an doubling in the methanol production. The productivity of the Co/Al₂O₃ catalyst is observed to increase nearly 5-fold but at the price of a decreased C—N cleavage selectivity.

3.3. Optimalization of catalyst support

While optimalization of the reactive temperature and residence time resulted in improvements in the methanol productivity and C—N cleavage selectivity in the previous sections for both catalysts, the methanol productivity remains low due to low C—N cleavage selectivity. While both the Au and Co active metals did not suffer from catalyst deactivation up to 3 hour time-on-stream, the methanol productivity per gram of active metal was observed to be approximately $20\times$ higher for the Au catalyst. Therefore, Au was selected as the active metal for further experiments.

Milstein et al. and Kothandaraman et al. reported that the addition of bases such as KOH and *t*-BuOK significantly enhances the methanol productivity over heterogenous catalysts [25,26]. This was rationalized through mechanistic studies, where it was shown that the initial hydrogenation of the formamide species occurs via the formation of a hemiaminal, with the addition of such bases facilitating the deprotonation of the intermediate hemiaminal, therefore retarding the cleavage of the C—O bond [26]. A schematic overview of the proposed reaction mechanism in acidic and basic conditions is given in Fig. 7.

While the addition of strong inorganic bases to formamides such as performed in the previously mentioned studies does not result in side-reactions occurring, upon the addition of strong inorganic bases such as KOH to a mixture of isopropanol and N-dipropylcarbamate a white precipitate was observed to form. FTIR spectroscopy revealed the precipitate to contain carbonates. Carbonates are practically insoluble in organic solvents, and therefore precipitation occurs. As such systems are not suitable for processing in fixed bed reactors, and the addition of highly corrosive inorganic bases would significantly complicate the downstream processing required to obtain high purity methanol, it was opted to focus on solid bases (MgO and ZnO) and amphoteric supports (TiO₂, CeO₂ and ZrO₂).

3.3.1. Determination of support surface acidity and basicity

To probe the Brønsted-acidity and basicity of the selected supports, the supports were characterized using NH₃ and CO₂ Temperature Programmed Desorption (TPD). An overview of the total amount of acid and base sites is given in Table 2, while the NH₃- and CO₂-TPD curves are given in Fig. 8. The total amount of acid and base sites was determined assuming each NH₃ or CO₂ molecule desorbs from a single site.

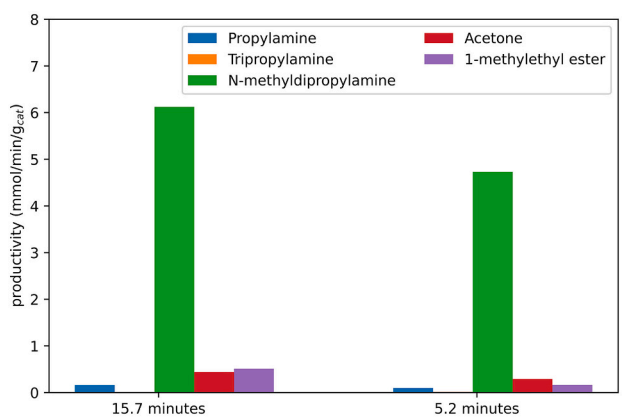


Fig. 3. Influence of residence time for a 1 wt% Au/TiO₂ catalyst at 135 °C. Left) Liquid and gas phase productivity, right) productivity of N-containing species, acetone and isopropyl ester. Experimental conditions: 2.0 g catalyst, 40 bar H₂ 135 °C, 10 vol% N,N-dipropylformamide in IPA.

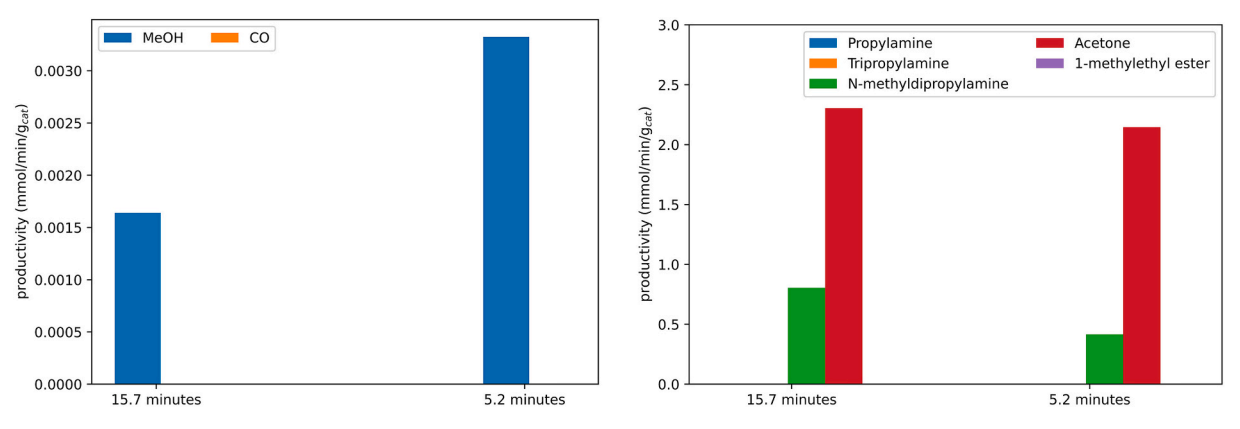


Fig. 4. Influence of residence time for a 40 wt% $Co(0)/Al_2O_3$ catalyst at 135 °C. Left) Liquid and gas phase productivity, right) productivity of N-containing species, acetone and isopropyl ester. Experimental conditions: 2.0 g catalyst, 40 bar H_2 , 135 °C, 10 vol% N,N-dipropylformamide in IPA.

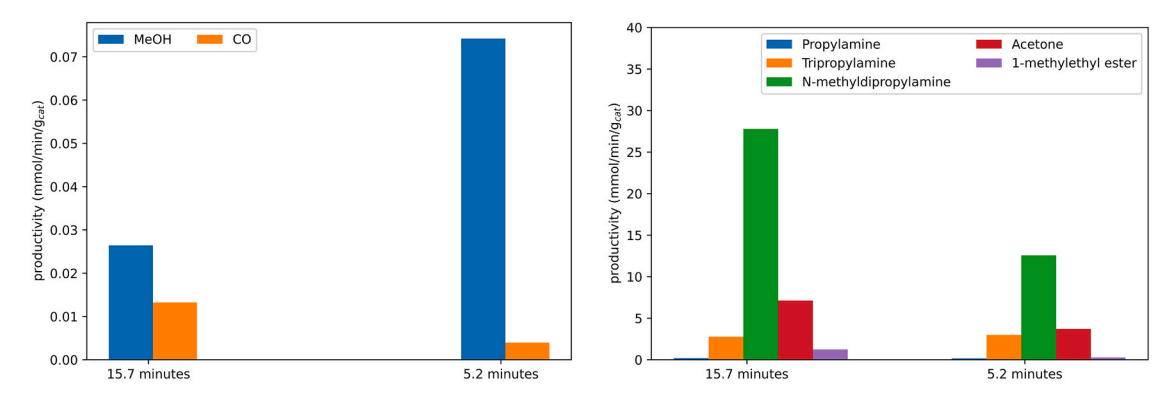


Fig. 5. Influence of residence time for a 1 wt% Au/ TiO_2 catalyst at 175 °C. Left) Liquid and gas phase productivity, right) productivity of N-containing species, acetone and isopropyl ester. Experimental conditions: 2.0 g catalyst, 40 bar H_2 , 175 °C, 10 vol% N,N-dipropylformamide in IPA. Change in residence time is achieved by changing the gas and liquid feed in equimolar ratio.

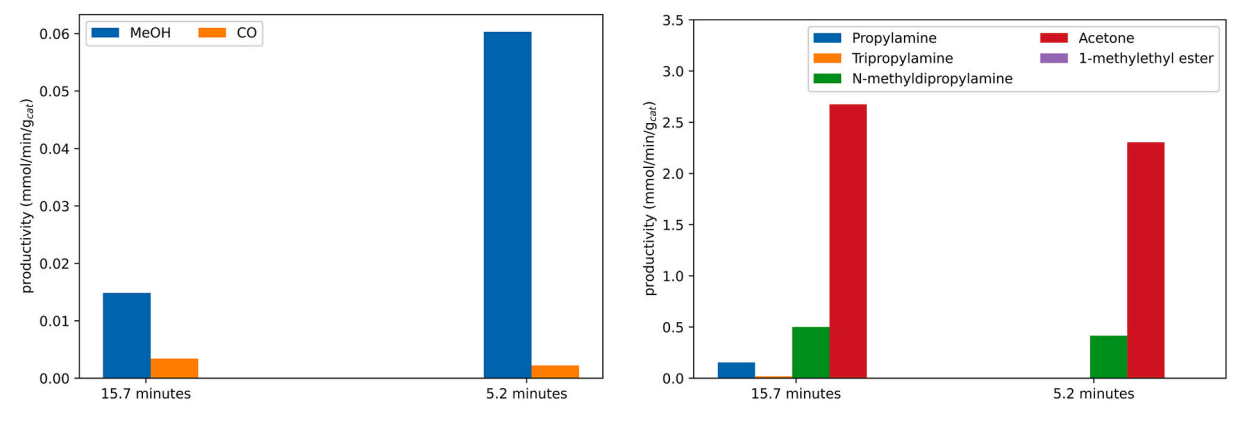


Fig. 6. Influence of residence time for a 40 wt% $Co(0)/Al_2O_3$ catalyst at 175 °C. Left) Liquid and gas phase productivity, right) productivity of N-containing species, acetone and isopropyl ester. Experimental conditions: 2.0 g catalyst, 40 bar $H_{2,}$ 175 °C, 10 vol% N,N-dipropylformamide in IPA. Change in residence time is achieved by changing the gas and liquid feed in equimolar ratio.

In Table 2 it is shown that the basic supports MgO and ZnO indeed contain the largest amount of basic sites of all supports studied, with 454 and 650 $\mu mol/g$ respectively. The amphoteric supports, TiO2, ZrO2 and CeO2 contain approximately 10 times less basic sites per $g_{support}$ at 280, 82 and 70 $\mu mol/g$, respectively. The amount of acid sites on the basic support is nearly negligible at 2.8 $\mu mol/g$ for the ZnO support and 61 $\mu mol/g$ for the MgO support, as well as for the ZrO2 support (18 $\mu mol/g$). CeO2 and TiO2 were observed to possess significant acidity, at 125 $\mu mol/g$ and 835 $\mu mol/g$.

The classification of the strength of an acidic site according to the

NH $_3$ -TPD desorption temperature is classified according to three categories. Here, desorption between 150 and 300 °C is assigned as weak acidic sites, 300–450 °C as moderate strength sites and desorption above as strong sites or the decomposition of ammonia based on the material [42,43]. Similar classifications were used for the strength of a basic site as determined by CO $_2$ -TPD, with weak basic sites being assigned for desorption temperatures below <300 °C, moderate 350–550 °C and strong >600 °C [44]. A detailed discussion of the observed CO $_2$ and NH $_3$ TPD results has been included within the S.I.

Fig. 7. Schematic overview of the proposed reaction mechanism in acidic and basic environments. Based on [25,26].

Table 2 Total amount of basic and acid sites for all studied catalyst supports, as determined by $\mathrm{NH_3}$ and $\mathrm{CO_2}$ TPD.

Catalyst	Amount of basic sites [µmol/g]	Amount of acid sites [µmol/g]
TiO ₂	280	835
ZrO_2	82	18
CeO_2	70	125
MgO	454	61
ZnO	650	2.8

3.3.2. Reactive testing of support Au-based catalysts

Based on the results presented in Section 3.1, the commercial Au/ TiO_2 catalyst was selected as the benchmark catalyst due to the much higher productivity per gram of active metal. Au-based catalysts were synthesized on the aforementioned MgO, ZnO, CeO₂ and ZrO₂ supports using deposition-precipitation technique. The catalysts were screened in flow using 10 vol% N,N-dipropylformamide in IPA as starting material

at a temperature of 135 $^{\circ}$ C and a residence time of 5.2 min, with results summarized in Tables 3 and 4. Additionally, the benchmark Au/TiO₂ catalyst is physically mixed with the studied supports to a homogeneous bed. No gaseous products such as CO₂, CO or CH₄ were observed for any of the studied catalysts at a reactive temperature of 135 $^{\circ}$ C.

From Table 3, a clear trend can be distinguished between the basicity and the C—N cleavage selectivity of the reaction. The catalysts possessing the same order of magnitude total amount of basic sites (MgO and ZnO) as the Au/TiO₂ catalyst remarkably improve the C—N cleavage selectivity compared to the benchmark Au/TiO₂ catalyst, while those possessing an order of magnitude less basic sites (CeO₂ and ZrO₂) are observed to have C—N cleavage selectivity slightly lower or comparable to those of the benchmark catalyst.

While the total amount of basic sites present on the TiO₂, MgO and ZnO is of the same order of magnitude, the strength of these basic sites differs significantly, as shown in the previous section through CO₂-TPD. While the TiO₂ mostly has a large number of weak basic sites, MgO was observed to possess mostly intermediate strength and a fraction of strong

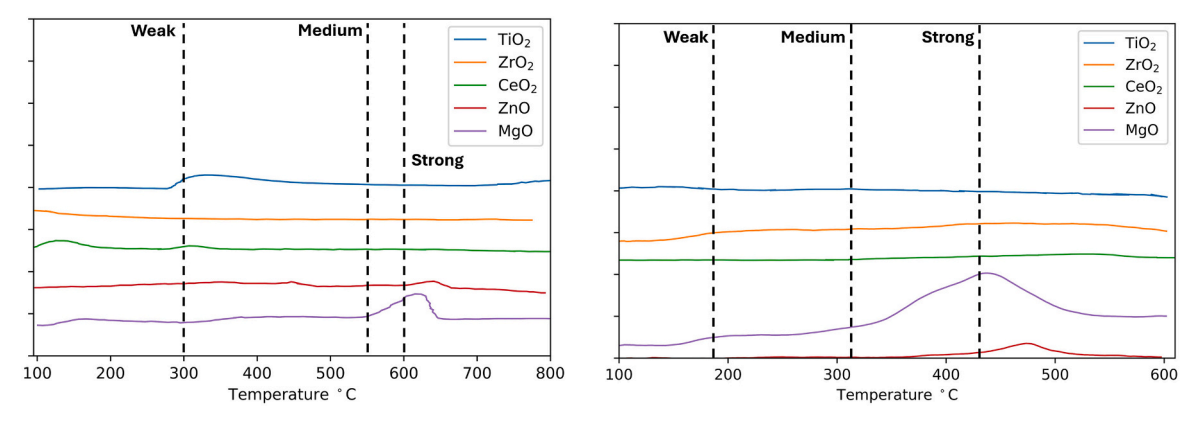


Fig. 8. CO₂ (left) and NH₃ (right) TPD of the different catalyst supports.

Table 3

Influence of the catalyst support material on methanol productivity and C—N cleavage selectivity at 135 °C. Experimental conditions: 2.0 g catalyst, 40 bar $\rm H_{2},$ 175 °C, 10 vol% N,N-dipropylformamide in IPA, residence time: 5.2 min. Au loading determined by ICP-OES. For the physical mixtures, 0.5 g support was mixed with 1.5 g Au/TiO $_{2}$.

Catalyst	Methanol productivity [mmol/l/g _{Au}]	C-N cleavage selectivity (%)
Au/TiO ₂	5.929	0.058
Au/ZrO ₂	2.927	0.051
Au/CeO ₂	2.547	0.041
Au/MgO	10.798	1.843
Au/ZnO	12.431	2.231
Au/TiO ₂ +	3.782	0.063
ZrO_2		
Au/TiO ₂ +	3.428	0.048
CeO_2		
Au/TiO ₂ +	8.564	1.112
MgO		
$Au/TiO_2 + ZnO$	9.752	1.709

Table 4 Influence of the catalyst support material on methanol productivity and C—N cleavage selectivity at 175 °C after 30 minute time-on-stream. Experimental conditions: 2.0 g catalyst, 40 bar $\rm H_{2,}$ 175 °C, 10 vol% N,N-dipropylformamide in IPA, residence time: 5.2 min. Au loading determined by ICP-OES. For the physical mixtures, 0.5 g support was mixed with 1.5 g Au/TiO $_2$.

Catalyst	Methanol productivity [mmol/l/ g_{Au}]	Produ	Product selectivity [carbon%]			
		CO	CH ₄	МеОН	DPA N- Me	
Au/TiO ₂	11.50	0.03	0	0.06	99.91	
Au/ZrO ₂	4.10	1.05	0	0.69	98.26	
Au/CeO ₂	3.88	0.02	0	0.66	99.32	
Au/MgO	0	0	0	0	100	
Au/ZnO	0	0	0	0	100	
$Au/TiO_2 + ZrO_2$	11.11	0.95	0	1.59	97.46	
Au/TiO ₂ + CeO ₂	10.80	0.03	0	0.34	99.63	
Au/TiO ₂ + MgO	11.43	0.04	0	0.07	99.89	
Au/TiO ₂ + ZnO	11.47	0.04	0	0.06	99.90	

basic sites while the ZnO support almost fully consist of strong basic sites. The C—N cleavage selectivity displays a similar trend, with the selectivity increasing from ${\rm TiO_2}$ to MgO to ZnO, thus according to the strength of the surface basicity.

Besides the increased basicity of the supports significantly enhancing the C—N cleavage selectivity, likely through the retardation of the rapid C—O cleavage pathway through the deprotonation of the hemiaminal intermediates, the methanol productivity per gram of deposited Au increases compared to the benchmark Au/TiO $_2$ catalyst is observed to increase according to the same trend.

Comparing the C—N cleavage selectivity and methanol productivity of the supported Au catalysts to the physical mixtures of basic materials with the benchmark Au/TiO $_2$ catalyst, similar trends are observed. Here, the addition of solid bases to the catalyst bed also significantly enhances both the C—N cleavage selectivity as well as the methanol productivity, however, to a lesser extent than observed for the synthesized materials. A possible explanation for this could be the decreased contact between the active gold site and the base required to deprotonate the hemiaminal intermediates. The experiments were repeated for a reactive temperature 175 °C, with results summarized in Table 4.

While the behavior of the $\rm ZrO_2$ and $\rm CeO_2$ systems is comparable to the previously observed trends, the performance of the MgO and ZnO systems does not follow the same trends. Contrary to the trends observed at 135 °C, the Au/MgO and Au/ZnO catalysts do not produce any

observable methanol after 30 minute time-on-stream.

Additionally, the physical mixtures of these basic catalyst supports result in similar C—N cleavage selectivity and methanol productivity as when solely using the benchmark Au/TiO_2 catalyst. The TOS curves of the physical mixtures compared to the commercial Au/TiO_2 catalyst are shown in Fig. 9.

Similarly to a reactive temperature of 135 $^{\circ}$ C, a significant enhancement of the methanol production is observed when ZnO or MgO are added to the catalyst bed. However, contrary to the lower reactive temperature, this enhancement is only present at the initial moments of the experiment, with severe catalyst deactivation observed at longer times-on-stream. Here, the methanol productivity is observed to decline until it converges to the performance of the Au/TiO₂ catalyst.

Typically, the deactivation of MgO and ZnO based catalysts in organic solvents such as methanol and isopropanol at elevated temperatures can be attributed to progressive lixiviation of the catalyst or poisoning of the active sites [46]. To assess the possibility of dissolution of the Mg or Zn ions, ICP-OES analysis of liquid samples taken during was performed. No Mg or Zn ions were detected, while the detection limit of the machine was established to be roughly 7 ppb in organic solvents. Therefore, the most likely cause of deactivation is poisoning of the active sites.

3.4. Proof-of-concept: carbamate hydrogenation

Previous work by Chila et al. [18] demonstrated that the hydrogenation of carbamates formed during carbon capture using secondary amines readily hydrogenate towards formamides, but that the subsequent hydrogenation into methanol is rate-limiting. Therefore, within Sections 3.1–3.3 the second reaction step was isolated from the complex mechanism by using N,N-dipropylformamide as a starting material, allowing us to gain further insight into process conditions and catalyst required to enable the hydrogenation of this compound. Within this section, the complete proposed process is demonstrated, thus starting from dipropylamine instead of N,N-dipropylformamide. Structural properties of the Au/TiO₂ and Pd/Al₂O₃ catalysts are reported elsewhere [18, 32]

Following the methodology developed in [18], carbamates were synthesized by bubbling CO_2 through dipropylamine at ambient conditions for 3 h. Saturation was verified using FTIR and was equal to 0.63 mol CO_2 /mol dipropylamine. Passing a 10 vol% carbamate solution (diluted in IPA) over the Au/TiO₂, Au/ZnO or Au/MgO catalyst at a residence time of 32 min, temperature of 175 °C and H_2 pressure of 40 bar did not yield any observable conversation towards N,N-

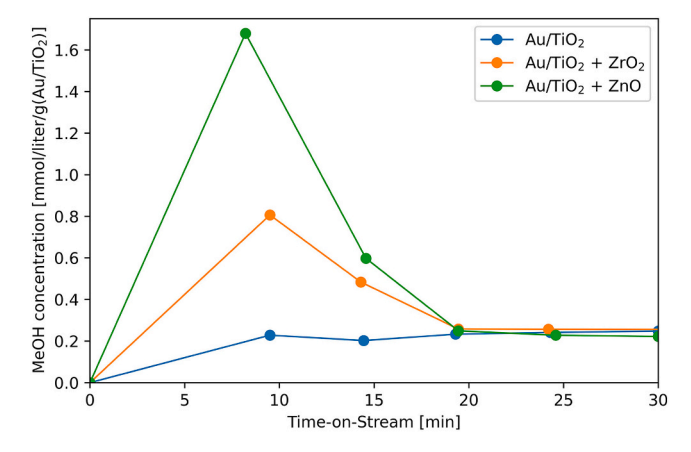


Fig. 9. Methanol productivity as function for several physical mixtures of 1 wt % Au/TiO_2 catalyst and a secondary basic catalyst. Experimental conditions: 2.0 g catalyst, 40 bar H_2 , 175 °C, 10 vol% N,N-dipropylformamide in IPA, residence time: 5.2 min. Au loading determined by ICP-OES. For the physical mixtures, 0.5 g support was mixed with 1.5 g Au/TiO_2 .

dipropylformamide. The reaction conditions were chosen based on the temperature, residence time and pressure trends presented in earlier work [18]. This previous work also highlighted the promising nature of using a 1 wt% Pd/Al $_2$ O $_3$ catalyst for the hydrogenation towards N,N-dipropylformamide. Repeating the experiment using a 1 wt% Pd/Al $_2$ O $_3$ and the aforementioned conditions resulted in the formation of a negligible (< 10 ppm) amount of methanol, 0.15 M N,N-dipropylformamide, 0.03 M tripropylamine and 0.015 M propylamine.

The inability of the gold-based catalysts to hydrogenate the N,N-dipropylcarbamate into N,N-dipropylformamide strongly underlines the difference in the reaction conditions and catalyst required to perform the hydrogenation towards formamides and the subsequent hydrogenation into methanol. Therefore, we propose a two-step process, in which the formation through carbon capture and hydrogenation of the carbamate into formamide takes place over a Pd-based catalyst in the first bed at high temperature and longer residence times, followed by hydrogenation of the formamide into methanol over an Au-based catalyst within the second bed at much lower temperatures and residence times. A visualization of the two-step configuration is given in Fig. 10.

To demonstrate this approach, the solution containing 0.15 M N,N-dipropylformamide in IPA formed using the Pd/Al $_2$ O $_3$ catalyst was used as a starting material for the second reaction step. Based on the results within this paper, the conditions were chosen to optimize the production of methanol: a reaction temperature of 135 °C, H $_2$ pressure of 40 bar and a residence time of 5.2 min. The benchmark Au/TiO $_2$ catalyst yielded a productivity of \sim 8.1 mmol/l/gAu of MeOH, while the productivity of the Au/ZnO was observed to be \sim 22.7 mmol/l/gAu.

To compare to the previously proposed system using dipropylamine, the 0.15 M N,N-dipropylformamide solution was passed over a second Pd/Al_2O_3 catalyst bed using a reactive temperature of 175 °C, H_2 pressure of 40 bar and a residence time of 21 min. These conditions were selected with the emphasis of optimizing the formation of methanol based on the work of Chila et al. [18]. This resulted in a methanol productivity 0.14 mmol/l/g_{Pd}. Decreasing the residence time to 5.2 min yielded a methanol productivity of 0.21 mmol/l/g_{Pd}.

Comparing the methanol productivity per gram of active metal of the Pd/Al_2O_3 and Au/ZnO catalyst, a significant enhancement of roughly a factor 100 in productivity is observed using the gold-based catalyst. Additionally, no deactivation of the Au/ZnO catalyst is observed up to 3 hour time-on-stream, while significant deactivation during this time period is reported in previous works for other noble metal catalysts based on common hydrogenation materials such as Pd, Pt and Ru [7,18].

While the final methanol concentrations remain low (\sim 10 mmol/l) under the studied conditions, the two-step strategy proposed within this work and the discovery of the Au/ZnO catalyst highlight the promising nature of the proposed reaction, even though significant further development are required prior to the proposed process becoming economically viable.

4. Conclusion

The combined carbon capture and hydrogenation towards methanol was demonstrated using dipropylamine as carbon capture agent. Initially, the process conditions and catalyst formulation were optimized using N,N-dipropylformamide as starting material. Several oxidation states of Co/Al $_2$ O $_3$ catalysts and an Au/TiO $_2$ catalyst were studied at a wide range of temperatures and residence times. Here, it was observed that only the zero valence oxidation state of Co and the Au/TiO $_2$ catalysts could catalyze the reaction at sufficient kinetic rates. Due to the methanol productivity of the Au-based catalyst being up to $20\times$ higher compared to the Co catalyst, it was opted to further develop Au-based catalysts.

Comparing Au/ZnO, Au/MgO, Au/CeO $_2$ and Au/ZrO $_2$ catalysts to the benchmark Au/TiO $_2$ catalyst, it was concluded that the methanol productivity strongly scales with the surface basicity of the catalyst support. This was rationalized in relation to the reaction mechanism, in

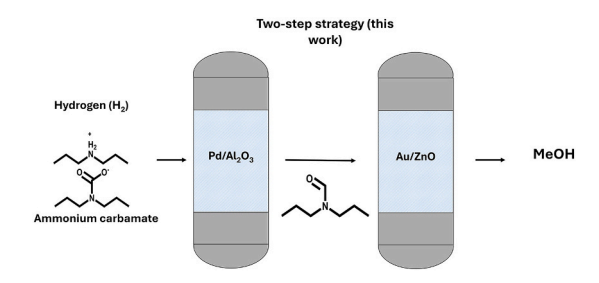


Fig. 10. Schematic overview of the current one-step strategy, and the newly proposed two-step process.

which the first hydrogenation step of the formamide species is proposed to occur via a hemiaminal intermediate. The deprotonation of the hemiaminal intermediate through the utilization of basic supports results in the retardation of C—O bond cleavage, effectively suppressing unwanted side reactions in the form of *N*-methylation and thus increasing methanol productivity and selectivity. The optimized reaction conditions and catalyst formulation were observed to be vastly different between the first (formation of N-formamide) and the second (methanol formation) reactions steps. To enable the optimal performance of both key reactive steps, a novel process configuration is designed within this work, in which two-sequential reactors are used instead of a single reactor.

Lastly, the novel processes configuration was demonstrated. In the two-step process, in which the formation through carbon capture and hydrogenation of the carbamate into formamide takes place over a Pd-based catalyst in the first bed at high temperature and longer residence times, followed by hydrogenation of the formamide into methanol over an Au-based catalyst within the second bed at much lower temperatures and residence times. Comparing the methanol productivity per gram of active metal of the state-of-the-art Pd/Al_2O_3 and Au/ZnO catalyst, a significant enhancement of roughly a factor 100 in productivity was observed using the novel gold-based catalyst and the two-step strategy proposed within this work.

CRediT authorship contribution statement

A. Chila: Writing – original draft, Visualization, Methodology, Investigation, Formal analysis, Data curation, Conceptualization. A.W. N. de Leeuw den Bouter: Writing – original draft, Visualization, Methodology, Investigation, Formal analysis, Data curation, Conceptualization. L. Brito: Writing – review & editing, Supervision, Methodology, Funding acquisition, Formal analysis, Conceptualization. A. Miquelot: Writing – review & editing, Supervision, Project administration, Methodology, Funding acquisition, Formal analysis, Conceptualization. P. Olivier: Writing – review & editing, Supervision, Project administration, Funding acquisition. J. van der Schaaf: Writing – review & editing, Supervision, Resources, Project administration, Methodology, Funding acquisition, Conceptualization.

Declaration of competing interest

The authors declare that they have no known competing financial interests or personal relationships that could have appeared to influence the work reported in this paper.

Acknowledgements

The funding for this work was provided by ENGIE Lab CRIGEN.

Appendix A. Supplementary data

Supplementary data to this article can be found online at https://doi.

org/10.1016/j.cej.2025.167680.

Data availability

Data will be made available on request.

References

- [1] C.D. Keeling, R.F. Keeling, Atmospheric monthly in situ CO₂ data Mauna Loa observatory, Hawaii (archive 2024-11-13), in: Scripps CO₂ Program Data, Collections, UC San Diego Library Digital, 2017, https://doi.org/10.6075/ JOBW3BHW
- [2] A. Buis, June 18, Getting a handle on carbon dioxide. NASA, The atmosphere, 2024 https://science.nasa.gov/earth/climate-change/greenhouse-gases/the-atmosphere-getting-a-handle-on-carbon-dioxide/.
- [3] D. Welsby, J. Price, S. Pye, P. Ekins, Unextractable fossil fuels in a 1.5 °C world, Nature 597 (2021) 230–234, https://doi.org/10.1038/s41586-021-03821-8.
- [4] H. Ritchie, Fossil fuels, Our World in Data, https://ourworldindata.org/fossil-fuels, 2024, August 10.
- [5] J. Kothandaraman, et al., Integrated capture and conversion of CO₂ to methane using a water-lean, post-combustion CO₂ capture solvent, ChemSusChem 14 (17) (2021) 4812–4819, https://doi.org/10.1002/cssc.202101590.
- [6] H. Fu, F. You, H. Li, L. He, CO₂ capture and in situ catalytic transformation, Front. Chem. 7 (2019) 525, https://doi.org/10.3389/fchem.2019.00525.
- [7] J. Kothandaraman, et al., Integrated capture and conversion of CO₂ to methanol in a post-combustion capture solvent: heterogeneous catalysts for selective c-n bond cleavage, Adv. Energy Mater. 12 (46) (2022) 2202369, https://doi.org/10.1002/ 2020.202369
- [8] A. Goeppert, M. Czaun, J.P. Jones, G.K. Surya Prakash, G.A. Olah, Recycling of carbon dioxide to methanol and derived products—closing the loop, Chem. Soc. Rev. 43 (23) (2014) 7995–8048, https://doi.org/10.1039/c4cs00122b.
- [9] X. Jiang, X. Nie, X. Guo, C. Song, J.G. Chen, Recent advances in carbon dioxide hydrogenation to methanol via heterogeneous catalysis, Chem. Rev. 120 (15) (2020) 7984–8034, https://doi.org/10.1021/acs.chemrev.9b00723.
- [10] J.R. Cabrero-Antonino, R. Adam, V. Papa, M. Beller, Homogeneous and heterogeneous catalytic reduction of amides and related compounds using molecular hydrogen, Nat. Commun. 11 (2020) 3893, https://doi.org/10.1038/ s41467-020-17588-5
- [11] G.A. Olah, Beyond oil and gas: the methanol economy, Angew. Chem. Int. Ed. 44 (18) (2005) 2636–2639, https://doi.org/10.1002/anie.200462121.
- [12] T.H. Ulucan, et al., Hydrogen storage in liquid hydrogen carriers: recent activities and new trends, Prog. Energy 5 (1) (2023) 012345, https://doi.org/10.1088/2516-1083/acac5c.
- [13] M. Ren, Y. Zhang, X. Wang, H. Qiu, Catalytic hydrogenation of CO₂ to methanol: A review. Catalysts 12 (4) (2022) 403. https://doi.org/10.3390/catal12040403.
- [14] G. Leonzio, N. Shah, Recent advancements and challenges in carbon capture, utilization and storage, Curr. Opin. Green Sustainable Chem. 46 (2024) 100895, https://doi.org/10.1016/j.cogsc.2024.100895.
- [15] D.J. Heldebrant, P.K. Koech, V. Glezakou, R. Rousseau, D. Malhotra, D.C. Cantu, Water-lean solvents for post-combustion CO₂ capture: fundamentals, uncertainties, opportunities, and outlook, Chem. Rev. 117 (14) (2017) 9635–9674, https://doi. org/10.1021/acs.chemrev.6b00768.
- [16] M.C. Freyman, et al., Reactive CO₂ capture: A path forward for process integration in carbon management, Joule 7 (4) (2023) 631–651, https://doi.org/10.1016/j. joule.2023.03.013.
- [17] D. Barpaga, et al., Single-pass demonstration of integrated capture and catalytic conversion of CO₂ from simulated flue gas to methanol in a water-lean carbon capture solvent, ACS Omega (2024), https://doi.org/10.1021/acsomega.4c06919.
- [18] A. Chila, A.W.N. de Leeuw den Bouter, A. Miquelot, P. Olivier, L. Brito, J. van der Schaaf, Integrated capture and conversion of CO₂ to methanol using dipropylamine: optimization of process conditions for amine stability, ACS Sustain. Chem. Eng. (2024) (Under review).
- [19] J. Kothandaraman, A. Goeppert, M. Czaun, G.A. Olah, G.K.S. Prakash, Conversion of CO₂ from air into methanol using a polyamine and a homogeneous ruthenium catalyst, J. Am. Chem. Soc. 138 (3) (2016) 778–781, https://doi.org/10.1021/ jacs.5b12354.
- [20] T.M. Rayder, E.H. Adillon, J.A. Byers, C.K. Tsung, A bioinspired multicomponent catalytic system for converting carbon dioxide into methanol autocatalytically, Chem 6 (7) (2020) 1742–1754, https://doi.org/10.1016/j.chempr.2020.04.008.
- [21] J.G. Uranga, et al., Methanol production from CO₂ via an integrated, formamide-assisted approach, Sustainable Energy Fuels 4 (4) (2020) 1773–1779, https://doi.org/10.1039/c9se01141b.

- [22] E. Balaraman, B. Gnanaprakasam, L.J.W. Shimon, D. Milstein, Direct hydrogenation of amides to alcohols and amines under mild conditions, J. Am. Chem. Soc. 132 (47) (2010) 16756–16758, https://doi.org/10.1021/ja1080019.
- [23] Y. Nakagawa, R. Tamura, M. Tamura, K. Tomishige, Combination of supported bimetallic rhodium-molybdenum catalyst and cerium oxide for hydrogenation of amide, Sci. Technol. Adv. Mater. 16 (1) (2015) 014901, https://doi.org/10.1088/ 1468-6996/16/1/014901.
- [24] I. Sorribes, S.C.S. Lemos, S. Martín, A. Mayoral, R.C. Lima, J. Andrés, Palladium doping of insO₃ towards a general and selective catalytic hydrogenation of amides to amines and alcohols, Cat. Sci. Technol. 9 (24) (2019) 6965–6976, https://doi.org/10.1039/c9cv02128k.
- [25] J. Kothandaraman, D.J. Heldebrant, J.S. Lopez, R.A. Dagle, Mechanistic insights to drive catalytic hydrogenation of formamide intermediates to methanol via deaminative hydrogenation, Front. Energy Res. 11 (2023) 1158499, https://doi. org/10.3389/fenrg.2023.1158499.
- [26] Y. Xie, P. Hu, T. Bendikov, D. Milstein, Heterogeneously catalyzed selective hydrogenation of amides to alcohols and amines, Cat. Sci. Technol. 8 (11) (2018) 2784–2788, https://doi.org/10.1039/c8cy00112j.
- [27] F. Barzagli, S. Lai, F. Mani, A new class of single-component absorbents for reversible carbon dioxide capture under mild conditions, ChemSusChem 8 (1) (2015) 184–191, https://doi.org/10.1002/cssc.201402421.
- [28] G. Manca, F. Barzagli, J. Nagy, M. Munzarová, M. Peruzzini, A. Ienco, Unraveling the mechanism and the role of hydrogen bonds in CO₂ capture by diluent-free amine sorbents through a combination of experimental and theoretical methods, Fuel 378 (2024) 132859, https://doi.org/10.1016/j.fuel.2024.132859.
- [29] G. Zhao, et al., Structure–activity relationships of Au/Al₂O₃ catalyst for the selective oxidative esterification of 1,3-propanediol and methanol, ChemistrySelect 4 (43) (2019) 12479–12490, https://doi.org/10.1002/slct.201903059.
- [30] H. Yazid, R. Adnan, M.A. Farrukh, S.A. Hamid, Synthesis of Au/Al₂O₃ nanocatalyst and its application in the reduction of p-nitrophenol, J. Chin. Chem. Soc. 58 (5) (2011) 593–601, https://doi.org/10.1002/jccs.201190093.
- [31] J.H. Yang, et al., Understanding preparation variables in the synthesis of au/Al₂O₃ using EXAFS and electron microscopy, Appl. Catal. Gen. 291 (2005) 73–84, https://doi.org/10.1016/j.apcata.2004.11.052.
- [32] de Leeuw den Bouter, A. W. N., Meijer, L. M. P., Miquelot, A., Brito, L., Oliver, P., & van der Schaaf, J., Effect of tertiary amine selection on CO₂ to formic acid hydrogenation with au-np catalyst, Ind. Eng. Chem. Res. (2025), https://doi.org/10.1021/acs.iecr.4c04902.
- [33] G.A. Filonenko, W.L. Vrijburg, E.J.M. Hensen, E.A. Pidko, On the activity of supported au catalysts in the liquid phase hydrogenation of CO₂ to formates, J. Catal. 343 (2016) 97–105, https://doi.org/10.1016/j.jcat.2015.10.002.
- [34] X.-L. Du, et al., Direct methylation of amines with carbon dioxide and molecular hydrogen using supported gold catalysts, ChemSusChem 8 (20) (2015) 3489–3496, https://doi.org/10.1002/cssc.201500486.
- [35] S. Liu, et al., Hetero-site cobalt catalysts for higher alcohols synthesis by CO₂ hydrogenation: a review, J. CO₂ Util. 67 (2023) 102322, https://doi.org/10.1016/j.jcou.2022.102322.
- [36] I.C. te Have, et al., Uncovering the reaction mechanism behind CoO as active phase for CO₂ hydrogenation, Nat. Commun. 13 (2022) 254, https://doi.org/10.1038/ s41467-022-27981-x.
- [37] Y. Lv, Y. Li, W. Shen, Synthesis of co_3O_4 nanotubes and their catalytic applications in CO oxidation, Catal. Commun. 42 (2013) 116–120, https://doi.org/10.1016/j.catcom.2013.08.017.
- [39] H. Qin, et al., Direct esterification of amides by the dimethylsulfate-mediated activation of amide C–N bonds, Commun. Chem. 7 (2024) 1180, https://doi.org/ 10.1038/s42004-024-01180-9.
- [40] H.N. Abdelhamid, M.N. Goda, A.E.A.A. Said, Selective dehydrogenation of isopropanol on carbonized metal–organic frameworks, Nano-Struct. Nano-Objects 24 (2020) 100605, https://doi.org/10.1016/j.nanoso.2020.100605.
- [41] E. Jasińska, B. Krzyżyńska, M. Kozlowski, Activated carbon modified with different chemical agents as a catalyst in the dehydration and dehydrogenation of isopropanol, Catal. Lett. 125 (1–2) (2008) 145–153, https://doi.org/10.1007/ s10562-008-9536-z.
- [42] A. Tresatayawed, P. Glinrun, B. Jongsomjit, Ethanol dehydration over WO₃/TiO₂ catalysts using titania derived from sol-gel and solvothermal methods, Int. J. Chem. Eng. 2019 (2019) 4936292, https://doi.org/10.1155/2019/4936292.
- [43] N. Vorobyeva, et al., Nanocrystalline ZnO(Ga): paramagnetic centers, surface acidity and gas sensor properties, Sens. Actuators B 182 (2013) 555–564, https:// doi.org/10.1016/j.snb.2013.03.068.
- [44] P. Du, T. Su, X. Luo, X. Xie, Z. Qin, H. Ji, Zr-modified ZnO for the selective oxidation of cinnamaldehyde to benzaldehyde, Catalysts 9 (9) (2019) 716, https:// doi.org/10.3390/catal9090716.
- [46] N. Oueda, Y.L. Bonzi-Coulibaly, I.W.K. Ouédraogo, Deactivation processes, regeneration conditions and reusability performance of CaO- or MgO-based catalysts used for biodiesel production—a review, Mater. Sci. Appl. 8 (1) (2017) 94–122, https://doi.org/10.4236/msa.2017.81007.